Magnetic excitations in the dipole-coupled singlet-singlet system HoF_3

1994 J. Phys.: Condens. Matter 6 505

(http://iopscience.iop.org/0953-8984/6/2/021)

J. Phys.: Condens. Matter 6 (1994) 505–522. Printed in the UK

Magnetic excitations in the dipole-coupled singlet–singlet system HoF_3

M J M Leask†, M R Wells†, R C C Ward†, S M Hayden‡ and J Jensen§

† Oxford Physics, Clarendon Laboratory, Parks Road, Oxford OX1 3PU, UK

‡ H H Wills Physics Laboratory, University of Bristol, Tyndall Avenue, Bristol BS8 1TL, UK and Institut Laue–Langevin, BP156X, 38042 Grenoble, France

§ Niels Bohr Institute, Ørsted Laboratory, Universitetsparken 5, 2100 Copenhagen, Denmark

Received 20 September 1993

Abstract. Well defined magnetic excitations in holmium trifluoride are observed in inelastic neutron-scattering experiments, both in the paramagnetic phase at 1.6 K and in the ferrimagnetic phase at 90 mK. The dispersion relations at the two temperatures have been determined along the high-symmetry directions, and the field dependence of the excitations has been studied at 1.6 K. These measurements and the previous studies of the magnetic properties of HoF_3 are analysed within the mean-field/random-phase approximation (RPA). The two lowest electronic states of Ho^{3+} ions are singlets, which are well separated from the remaining levels. The dominating coupling between the ions is the classical dipole interaction, which forces the system to order at $T_C = 0.53$ K. The two-ion coupling is below the threshold value for inducing the ordering of the electronic system; it only occurs because the magnetic susceptibility is enhanced by the hyperfine interaction between the electronic and nuclear moments on the Ho ions. The classical dipole coupling is calculated directly from first principles, whereby the response function is nearly fixed by the macroscopic properties of the system. The calculated response is found to agree accurately with the observations in the paramagnetic phase, whereas some discrepancies occur in the ordered phase. These may indicate that correlation effects beyond the RPA are important or that two-ion (magnetoelastic) quadrupole couplings are present.

1. Introduction

The magnetic properties of holmium trifluoride have been discussed in two previous publications. Bleaney *et al* (1988) carried out optical and NMR experiments, and from these and measurements of the magnetic susceptibility and heat capacity they concluded that HoF_3 orders at 0.53 K. Brown *et al* (1990) determined the magnitude and direction of the Ho moments in the ordered state by neutron diffraction. They found that the ordered moments have a ferromagnetic component along the a axis and an antiferromagnetic one along the c axis. In this third paper we report a comprehensive study of the magnetic excitations both in the paramagnetic and in the ordered phase, and we present a coherent description of the magnetic properties of HoF_3 based on all the experimental material.

HoF_3 belongs to the orthorhombic space group $Pnma$. The lattice parameters are $a = 0.6404$ nm, $b = 0.6875$ nm and $c = 0.4379$ nm, and one unit cell contains four Ho^{3+} and 12 F^- ions. Due to the low symmetry at the Ho sites, the $J = 8$ ground-state multiplet splits into singlets, and below about 5 K the magnetic properties are determined almost exclusively by the ground and first excited states. This means that the low-temperature susceptibility of a single Ho ion is extremely anisotropic, being very small along the directions perpendicular to the easy axis. In this sense the system may be considered

0953-8984/94/020505+18$07.50

to be an Ising system. However, there are two magnetically easy directions, one for each pair of Ho ions in the unit cell. The two easy axes are both perpendicular to the b axis and make angles $+\theta$ and $-\theta$ with the a axis. In the ordered phase the moments are constricted to be along these two directions, and the diffraction measurements by Brown *et al* (1990) determined the angle θ to be $\pm 24°$ with $1°$ accuracy.

The dipole coupling between the angular moments on nearest Ho neighbours is about 0.002 meV, but although weak this classical dipole coupling is found to be one order of magnitude stronger than any other interactions between the dipoles. The classical dipole coupling gives rise to strong correlation effects below 5 K and is responsible for the induced magnetic ordering of the singlet ground-state system at T_C, which makes it a unique system. The two-ion coupling in HoF_3 is however not sufficiently strong to produce an ordering of the electronic system by itself. The ratio R between the two-ion coupling and the threshold value required for inducing magnetic ordering of the electronic moments is found to be $R = 0.86$. This is similar to praseodymium metal, as discussed for instance in the review of Jensen and Mackintosh (1991), and as in this case the hyperfine interaction between the electronic moments and the nuclear spin produces a cooperative ordering of the coupled systems at sufficiently low temperature.

The experimental details are presented in section 2. The macroscopic properties of HoF_3 are analysed within the mean-field approximation in section 3. In the following section, the result of this analysis is then used as a basis for an interpretation of the magnetic excitation spectrum using the random-phase approximation (RPA). Our conclusions and a general discussion of the magnetic properties of HoF_3 are presented in section 5.

2. The experiments

Single crystals of HoF_3 were grown by the Czochralski pulling technique under a reactive (HF) atmosphere. The crystals, which were seeded along the orthorhombic a, b and c axes, were typically 12 mm in diameter and 30 mm long and grown from platinum crucibles using RF heating. Pulling rates of 5–10 mm h^{-1} and rotation rates of 60–80 RPM were employed. Because of the anisotropy of the crystal structure, the crystal cross-section was not perfectly circular; in some cases a regular cylinder was prepared by ultrasonic trepanning, in order to provide a constant cross-section sample as seen by the neutron beam.

Three crystals used in the experiments were prepared for mounting so that their vertical axes were parallel to either the a, b or c axis. A dilution refrigerator was utilised with a base temperature of 50 mK, and the cryostat also contained a superconducting solenoid capable of providing vertical fields up to a maximum of 6 T.

In this paper we report a study of the magnetic excitations in HoF_3 both above and below T_C, using inelastic neutron scattering. These excitations were studied using the cold-source triple-axis spectrometer IN12 at the Institut Laue–Langevin, Grenoble. A vertically curved pyrolitic graphite (0 0 2) monochromator and analyser were used with a collimation of open–60′–60′–60′, and a cooled beryllium filter was placed in the scattered beam.

Figure 1 shows typical high-resolution scans performed with fixed $k_f = 1.2$ Å^{-1}. Somewhat broad excitation peaks develop around 4 K. The peaks narrow as the temperature is reduced. At 1.6 K (see figure 2), which is still in the paramagnetic regime, the widths are comparable to the experimental resolution width (0.08 meV). At this temperature, the energies of the magnetic excitations were measured along all three high-symmetry directions, and the scattering peak at (0 0 1) was measured as a function of field applied along the a-direction. In the ordered phase, the dispersion relation was studied at 90 mK, at which temperature the moments are near their zero-temperature value.

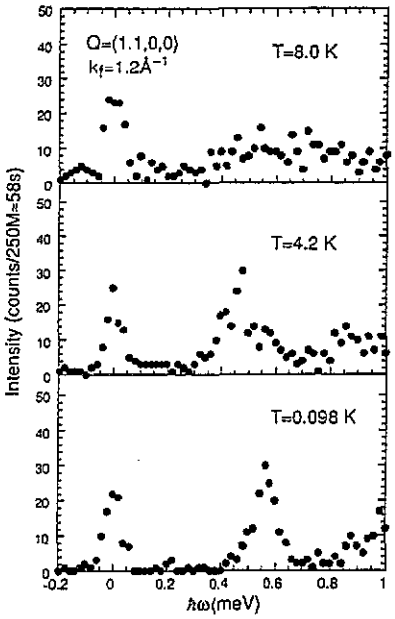

Figure 1. Constant-Q=(1.1,0,0) scans for various temperatures in HoF_3. The data were collected with a collimation of open–60′–60′–60′ and a fixed final wave-vector $k_f = 1.2$ Å^{-1}, giving an instrumental resolution of 0.08 meV. It can be seen that the excitation near 0.5 meV develops and becomes sharper on cooling (see also figure 2).

Most of the inelastic scattering occurs below about 1 meV. However, nearly all scans that were extended to higher energies showed an additional scattering peak. The extra peak behaves very similarly at 1.6 K and 90 mK, showing very little dispersion. The energy was near 1.4 meV in all the scans and the intensity was quite constantly about one tenth of the intensity of the main peaks. Figure 3 shows scans at 1.6 K made up to higher energy transfer with $k_f = 1.5$ Å^{-1}. The extra peak is clearly visible in these scans obtained at three different Bragg points. The figure illustrates the very strong polarization dependence of the inelastic-scattering intensities of the main peaks. This contrasts with the behaviour of the intensity of the extra peak, which is roughly the same in the three scans.

3. The mean-field model

The details of the orthorhombic structure of HoF_3 are discussed in the preceding papers, and figure 4 shows the projection of the ions in one unit cell on planes perpendicular to the b and the c axis. The four Ho sublattices are labelled by the numbers 1–4. The surroundings of the sites 1 and 2, or the sites 3 and 4, are the same, subject to a rotation by 180° around the b axis, whereas the sites 1 and 3, or 2 and 4, are equivalent after a reflection in the plane perpendicular to the c axis. In combination with the mirror plane symmetry perpendicular to the b axis, this means that the crystal-field Hamiltonian for all the four different sites is the same when referring to one local coordinate system for the sublattices 1 and 2 and another, in which the b and the c axis are reversed, for the sublattices 3 and 4.

The crystal-field Hamiltonian of the Ho ions has been determined by Sharma *et al* (1981) and Ram and Sharma (1985) by optical experiments. The most important feature

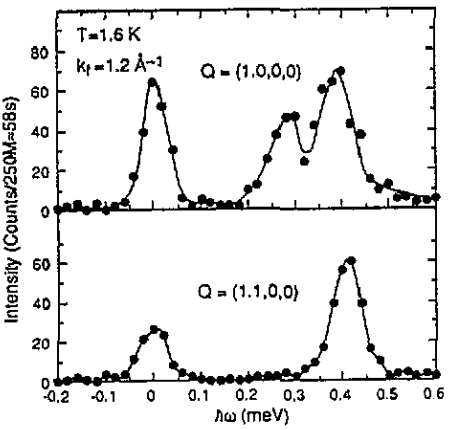

Figure 2. Constant-wave-vector scans near the $Q = (1, 0, 0)$ position. The lower peak at about 0.29 meV is present only near $Q = (1, 0, 0)$. The singular behaviour of the excitations close to the Bragg points is a consequence of the long range of the magnetic dipole interaction (see section 4).

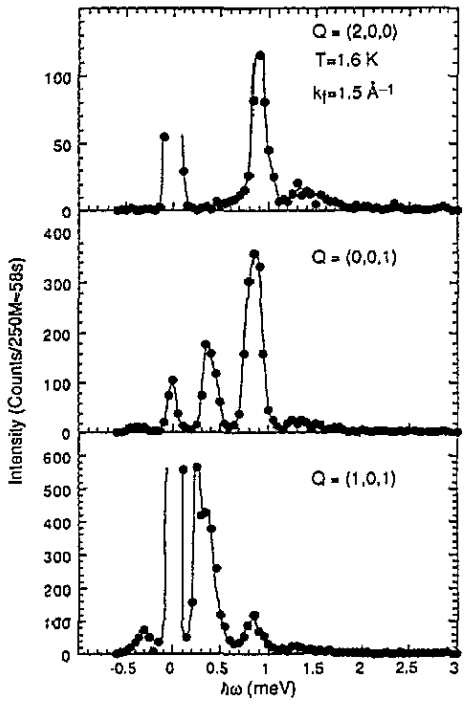

Figure 3. Constant-wave-vector scans at three different Bragg points. k_f is set equal to 1.5 Å^{-1} to enable higher energy transfers to be reached, in which case the experimental resolution is 0.18 meV. Notice the use of different intensity scales in the three cases.

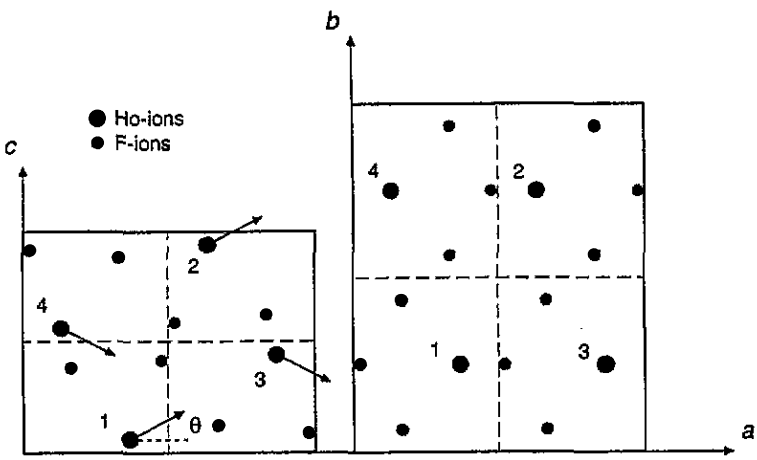

Figure 4. The four Ho and 12 F ions in one unit cell of the orthorhombic structure of HoF_3 projected on the a–c and the a–b plane. The arrows indicate the easy directions (or the x axes) lying in the a–c plane, making the angles $+\theta$ or $-\theta$ with the a axis. The arrows also show the directions of the moments in the ordered phase, assuming that $\theta = +25°$.

of the resulting level scheme is that the low-temperature properties are dominated by the ground state and the first excited state. The energy difference Δ is 0.85 meV in the model of Sharma *et al* and the magnetic dipole matrix element between the two states is large. The next excited state lies at about 5 meV, and the remaining 14 states between 10 and 50 meV above the ground state. This arrangement of the crystal-field levels leads to a very anisotropic susceptibility at low temperatures. The easy axis is perpendicular to the b axis of the crystal, but the optical experiments did not specify its direction within the a–c plane. Defining the easy axis of the different ions to be the local x axis, making the angles $+\theta$ and $-\theta$ with the a axis as indicated in figure 4, then the only parameters of importance in the present context are:

(i) the singlet–singlet energy difference Δ;
(ii) the direction of the x axis, i.e. θ, and
(iii) the numerical value, M, of the J_x matrix element between the singlets.

Utilising the level scheme of Sharma *et al* (1981), shown in their table III, as the starting point we fitted the low-temperature properties of HoF_3 by varying the three parameters listed above. Fortunately, the next excited level lies so high that the low-temperature heat capacity is dominated by the Schottky anomaly due to the lowest excited singlet, and as shown in figure 5 the position of the maximum is very well described with $\Delta = (0.71 \pm 0.02)$ meV. The modified value of Δ was obtained from that of Sharma *et al* by scaling their parameters $B^6_{\pm 2}$ by the factor 0.93, and the final crystal-field Hamiltonian is

$$\mathcal{H}_{CF} = \sum_j \sum_{l=2,4,6} \left(V_{l0} \tilde{O}_{l0}(j) + \sum_{m=2,4,6} \left[V_{lm} \tilde{O}_{lm}(j) + V^*_{lm} \tilde{O}_{l-m}(j) \right] \right) \qquad (1)$$

defined in terms of the Racah operators. The z axis is along the b direction of the crystal and the (local) low-temperature easy axis is the x axis (very nearly defined by the requirement that only J_x has a non-zero matrix element between the two lowest singlets). Table 1 gives the values of the crystal-field parameters in this coordinate system.

Table 1. Crystal-field coupling parameters (meV).

m	0	2	4	6
$V_{2m} \times 10^2$	-1.98	$-8.24 + i2.23$	—	—
$V_{4m} \times 10^4$	-0.69	$-2.26 - i3.45$	$-5.84 - i9.14$	
$V_{6m} \times 10^5$	-3.35	$6.48 - i4.63$	$-0.89 - i0.69$	$2.22 - i5.64$

The two other parameters θ and M are determined by the magnetization curves; the saturation values of $\langle J_\parallel \rangle$ in the cases where the field is applied along the a or the c directions are respectively $M\cos\theta$ and $M\sin\theta$. Figure 6 shows the calculated magnetization curves, at 1.6 K and 4.2 K, compared with the experiments of Bleaney *et al* (1988). In the calculations, the parameters of table 1 are used with $\theta = 25°$ and one ferromagnetic two-ion coupling constant. The latter is only important for the low-field behaviour and is, as we shall see below, very nearly determined alone by the classical dipole–dipole coupling. We may conclude here that the high-field magnetization is rather well determined with $M = 6.54$ (the value predicted by the parameters in table 1) and $\theta = 25°$, corresponding to the saturation moments $7.41\mu_B$ and $3.45\mu_B$. The moments do not however really saturate at these values because of a slight admixture of the higher-lying levels induced by the

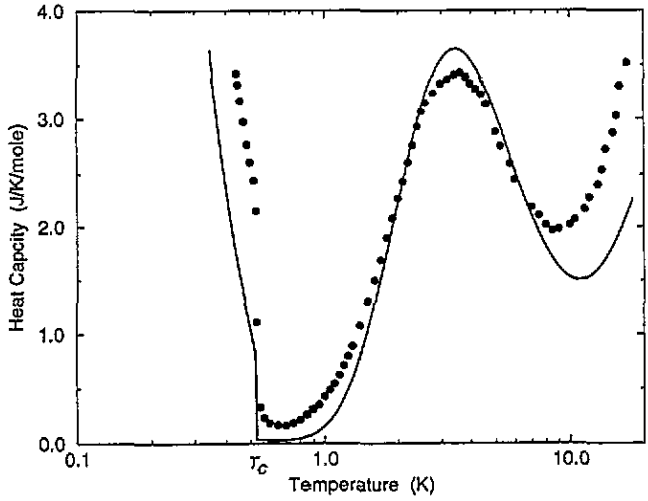

Figure 5. The low-temperature heat capacity of HoF_3. The solid circles are the experimental results obtained by Bleaney *et al* (1988), and the solid line is the magnetic contribution predicted by the mean-field theory. The heat capacity is calculated to be non-zero just above T_C due to the quadrupole splitting of the nuclear spin states. The difference between theory and experiment above 8 K is of a magnitude that may be accounted for by the phonons.

field. The three effective crystal-field parameters plus the same exchange-coupling constant also determine the susceptibility. The exchange-coupling constant was adjusted so that the calculated transition temperature agrees with the observed T_C=0.53 K. The comparison between the calculated and measured *aa*-susceptibility component, which diverges at T_C, is shown in figure 7. The two other components are small and nearly constant above T_C. The values of the *bb* and *cc* components measured by Bleaney *et al* (1988) at 1.6 K are respectively 0.09 and $0.12\mu_B$ kOe^{-1} per Ho ion, whereas the calculated values are 0.06 and $0.16\mu_B$ kOe^{-1}. The *bb* component derives from the coupling between the ground state and the second excited singlet. That this calculated component is somewhat smaller than observed may reflect the fact that the second excited state, at about 5.6 meV in the present model, lies too high. Sharma *et al* (1981) found indications of this level at 4.7 meV. We have tried to change the crystal-field parameters so to place the first excited state at 0.71 meV and the second one near to that observed by Sharma *et al* The only consequence of the modified model is found to be that the calculated *bb* component is increased to become close to the observed value. However, this improvement requires rather more extensive changes of the crystal-field Hamiltonian than the present model, and because our only claim is that the three parameters listed above are determined from the present analysis, we refrained from this modification. The discrepancy between the calculated and observed value of the *cc* component is a little surprising, when compared with the good fit obtained to the *c*-axis magnetization curve at 4.2 K shown in figure 6.

In all the calculations above we have included the effects of the nuclear spins on the Ho ions. If the hyperfine coupling between these spins and the 4f electrons on the Ho ions were neglected, the system would be undercritical, showing no phase transition. The effects of the hyperfine interaction on singlet ground-state systems is discussed by Jensen and Mackintosh (1991), to which we refer for the details of the following discussion. The hyperfine interaction is

$$\mathcal{H}_{hf} = A\, I \cdot J \tag{2}$$

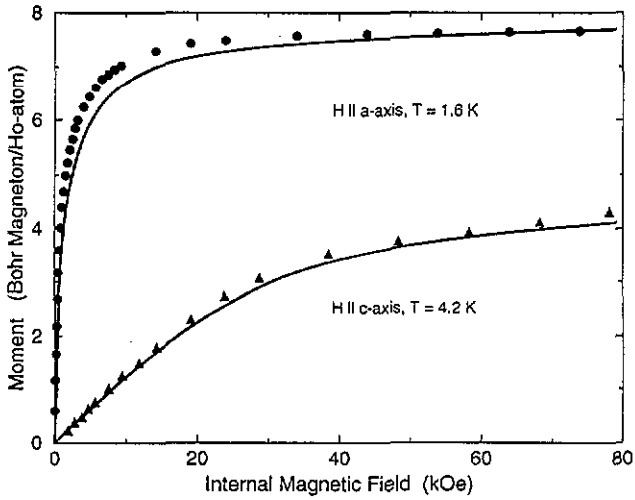

Figure 6. The magnetic moment of HoF_3 as a function of field along the a axis at 1.6 K and along the c axis at 4.2 K. The experimental results of Bleaney *et al* (1988) have been corrected for the demagnetization field estimated from the shape of the samples. The mean-field predictions are shown by the solid lines.

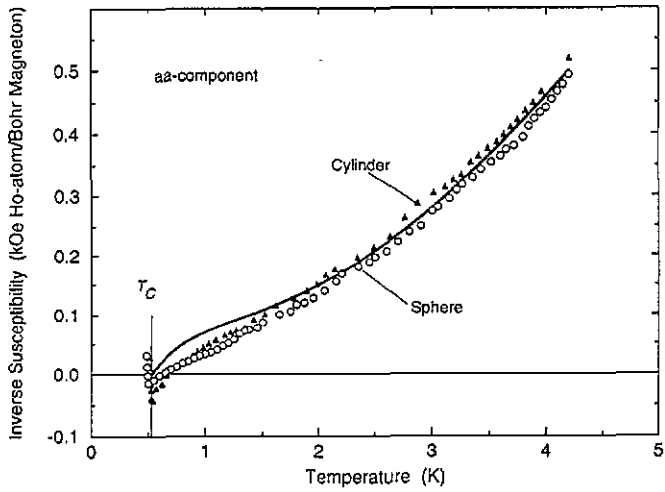

Figure 7. The reciprocal aa-component of the susceptibility as a function of temperature. Bleaney *et al* (1988) performed experiments on samples of different shapes, and the demagnetization factors d used for determining the internal response were 0.333 and 0.210 in the cases of the sphere and the cylinder respectively. The d factor for the cylinder is adjusted slightly (reduced by about 0.01) compared to that derived from the corresponding ellipsoidally shaped sample. The solid line shows the calculated behaviour.

where $A = 3.36 \times 10^{-3}$ meV and $I = \frac{7}{2}$ for the Ho ions, as specified by Bleaney (1972). A perturbation calculation leads to the following effective Hamiltonian:

$$\mathcal{H}_{\rm hf}({\rm eff}) = A\langle I\rangle \cdot (J - \tfrac{1}{2}\langle J\rangle) + A\langle J\rangle \cdot (I - \tfrac{1}{2}\langle I\rangle) - \tfrac{1}{2}A^2 (I - \langle I\rangle) \cdot \overline{\overline{\chi}}^0 \cdot (I - \langle I\rangle) \quad (3)$$

where $\overline{\overline{\chi}}^0$ is the zero-frequency mean-field susceptibility of the angular moments (the usual

mean-field suscptibility divided by $(g\mu_B)^2$). Introducing $\overline{\overline{\chi}}_I$ as the susceptibility tensor of the nuclear spins, we may write the resulting effective susceptibility as

$$\overline{\overline{\chi}}^0_{\text{eff}} = \overline{\overline{\chi}}^0 + A^2 \overline{\overline{\chi}}^0 \cdot \overline{\overline{\chi}}_I \cdot \overline{\overline{\chi}}^0 \tag{4}$$

where the $\alpha\alpha$ component of $\overline{\overline{\chi}}_I$ in the paramagnetic phase, when $\langle J \rangle = 0$, is approximately

$$\chi_I^{\alpha\alpha} = \frac{I(I+1)}{3k_B T}\left[1 + \frac{A^2}{15k_B T}\left(3\chi^o_{\alpha\alpha} - \sum_\gamma \chi^o_{\gamma\gamma}\right)\right]. \tag{5}$$

The final contribution to the mean-field Hamiltonian derives from the two-ion coupling

$$\mathcal{H}_{\text{dd}} = -\frac{1}{2}\sum_{ij}\sum_{\alpha\beta} \mathcal{J}^{\alpha\beta}(ij) J_{i\alpha} J_{j\beta} \tag{6}$$

which is assumed to be a sum of an isotropic exchange term plus the classical magnetic dipole–dipole interaction

$$\mathcal{J}^{\alpha\beta}(ij) = \delta_{\alpha\beta}\mathcal{J}(ij) + D^{\alpha\beta}(ij)\mathcal{J}_D \tag{7}$$

$D^{\alpha\beta}(ij)$ is the dimensionless coupling parameter

$$D^{\alpha\beta}(ij) = \frac{3(R_{i\alpha} - R_{j\alpha})(R_{i\beta} - R_{j\beta}) - |\boldsymbol{R}_i - \boldsymbol{R}_j|^2}{|\boldsymbol{R}_i - \boldsymbol{R}_j|^5} v_u \tag{8a}$$

and, recalling that the magnetic moment of the ith ion is $g\mu_B \boldsymbol{J}_i$ and $v_u = V/N$ is the volume V divided by the number of unit cells N, we have

$$\mathcal{J}_D = (g\mu_B)^2/v_u = 0.435 \times 10^{-3} \text{ meV} \tag{8b}$$

in HoF_3. We wish to calculate the spatial Fourier transforms of the two-ion couplings between the four different sublattices (r, s)

$$\mathcal{J}^{\alpha\beta}_{rs}(q) = \frac{1}{N}\sum_{i\in r}\sum_{j\in s} \mathcal{J}^{\alpha\beta}(ij)\, e^{-iq\cdot(\boldsymbol{R}_i - \boldsymbol{R}_j)}. \tag{9}$$

The Fourier transforms of $D^{\alpha\beta}(ij)$ were calculated using the Ewald method as refined by Bowden and Clark (1981). The results derived by their method were checked in various ways and appeared to be trustworthy.

The system is complex and there are 4×4 of the 3×3 coupling matrices. This number may be reduced by symmetry,

$$\begin{aligned} &\overline{\overline{\mathcal{J}}}_{rs}(q) = \{\overline{\overline{\mathcal{J}}}_{sr}(q)\}^* = \overline{\overline{\mathcal{J}}}_{sr}(-q) \qquad \overline{\overline{\mathcal{J}}}_{rr}(q) = \overline{\overline{\mathcal{J}}}_{ss}(q) \\ &\overline{\overline{\mathcal{J}}}_{23}(q) = \overline{\overline{\mathcal{J}}}_{41}(q) \qquad \overline{\overline{\mathcal{J}}}_{24}(q) = \overline{\overline{\mathcal{J}}}_{31}(q) \end{aligned} \tag{10}$$

and $\overline{\overline{\mathcal{J}}}_{34}(q)$ and $\overline{\overline{\mathcal{J}}}_{12}(q)$ are closely related (they are equal if all the c components in $\overline{\overline{\mathcal{J}}}_{12}$ and in its argument q are reversed).

Because of the very long range of the dipole coupling, its Fourier transform changes rapidly at small wave-vectors, as discussed for example by Jensen and Mackintosh (1991). If the wave-vector is identically zero the result may be written

$$\tilde{D}^{\alpha\beta}_{rs}(\mathrm{o}) = \left[D^{\alpha\beta}_{rs}\right]_{\mathrm{L}} + \delta_{\alpha\beta}\left(\frac{4\pi}{3} - N_\alpha\right) \tag{11}$$

The first term is the lattice-sum contribution, the next is the Lorentz term, and the last the demagnetization term. $N_\alpha = \frac{4\pi}{3} d_\alpha$, where d_α is the demagnetization factor, lying between zero and unity, and $d_1 + d_2 + d_3 = 1$. Equation (11) is valid for a uniformly magnetized crystal, which only occurs in the presence of an applied field H_{A} (along the α-axis) larger than the demagnetization field $H_{\mathrm{D}} = N_\alpha \langle (4N/V) g \mu_{\mathrm{B}} \langle J_\alpha \rangle \rangle_{\mathrm{crystal}}$, or in terms of the internal field $H_{\mathrm{I}} \equiv H_{\mathrm{A}} - H_{\mathrm{D}}$, when H_{I} is non-zero. In this case, the Hamiltonian is unchanged if N_α is neglected in (11) and H_{A} is replaced by H_{I} in the Zeeman term. If the crystal is ordered at zero field, the average magnetization density near the surface is nevertheless zero, because of the domains, and the demagnetization term is absent. This means that, if H_{A} is replaced by H_{I} in the Hamiltonian, (nearly) all effects of the demagnetization term are accounted for (the energy due to the domain walls is neglected), in which case the dipole coupling is

$$D^{\alpha\beta}_{rs}(\mathrm{o}) = \left[D^{\alpha\beta}_{rs}\right]_{\mathrm{L}} + \delta_{\alpha\beta}\frac{4\pi}{3}. \tag{12}$$

At non-zero, but very small, wave-vectors, the result is

$$D^{\parallel}_{rs}(q \to \mathrm{o}) = \left[D^{\parallel}_{rs}\right]_{\mathrm{L}} - \frac{8\pi}{3} = D^{\parallel}_{rs}(\mathrm{o}) - 4\pi \tag{13}$$

for the component parallel to q, whereas for the two transverse components

$$D^{\perp}_{rs}(q \to \mathrm{o}) = \left[D^{\perp}_{rs}\right]_{\mathrm{L}} + \frac{4\pi}{3} = D^{\perp}_{rs}(\mathrm{o}). \tag{14}$$

Hence the result is that the longitudinal component of $D^{\alpha\beta}_{rs}(q)$ immediately jumps by -4π when the wave-vector becomes non-zero, whereas all other components stay unchanged (also the non-diagonal ones).

The global coordinate system has axes along the a, b, and c directions of the crystal. If we use this system, but reverse the c components of the moments on the sublattices 3 and 4, assimilating the sign changes in the coupling constants (indicated by primes) then the four (3×3)-matrix eigenvalues of the coupling matrix may be written

$$\begin{aligned}
\overline{\overline{A}}_1 &= \overline{\overline{J}}_{11}(\mathrm{o}) + \overline{\overline{J}}_{12}(\mathrm{o}) + \overline{\overline{J}}'_{13}(\mathrm{o}) + \overline{\overline{J}}'_{14}(\mathrm{o}) \\
\overline{\overline{A}}_2 &= \overline{\overline{J}}_{11}(\mathrm{o}) - \overline{\overline{J}}_{12}(\mathrm{o}) + \overline{\overline{J}}'_{13}(\mathrm{o}) - \overline{\overline{J}}'_{14}(\mathrm{o}) \\
\overline{\overline{A}}_3 &= \overline{\overline{J}}_{11}(\mathrm{o}) + \overline{\overline{J}}_{12}(\mathrm{o}) - \overline{\overline{J}}'_{13}(\mathrm{o}) - \overline{\overline{J}}'_{14}(\mathrm{o}) \\
\overline{\overline{A}}_4 &= \overline{\overline{J}}_{11}(\mathrm{o}) - \overline{\overline{J}}_{12}(\mathrm{o}) - \overline{\overline{J}}'_{13}(\mathrm{o}) + \overline{\overline{J}}'_{14}(\mathrm{o}).
\end{aligned} \tag{15}$$

The largest contribution of the dipole coupling appears in $\overline{\overline{A}}_1$,

$$\sum_s \overline{\overline{D}}^{(\mathrm{o})}_{1s} = \begin{pmatrix} 19.871 & 0 & -0.487 \\ 0 & 15.778 & 0 \\ -0.487 & 0 & 5.037 \end{pmatrix} \tag{16}$$

and the maximum value of this coupling in the a–c plane occurs at $\theta = -1.9°$. The non-zero value of θ, which derives from the non-diagonal term in (16), introduces a weak asymmetry between the cases where θ is positive or negative. The sign of θ was not determined in the neutron diffraction experiment, and because the asymmetry is weak the present analysis gives no indication of which sign is correct.

The crystal-field Hamiltonian confines the moments to be along the x directions specified by θ. There are two possible values of this angle, $\theta = \pm 25°$, and in the case where $\theta = +25°$ the effective coupling parameter is

$$\mathcal{J}_1(\theta) = A_1^{11}\cos^2\theta + A_1^{33}\sin^2\theta + A_1^{13}\sin 2\theta = 2\mathcal{J}_{13}\cos 2\theta + 2\mathcal{J}_{12} + 16.848\mathcal{J}_D. \tag{17}$$

$\mathcal{J}_{13}$ and $\mathcal{J}_{12}$ are the inter-ionic exchange coupling constants between nearest and next-nearest neighbours respectively. The component χ^o_{xx} along this direction is calculated to be 120.7 meV^{-1} in the low-temperature limit, corresponding to an effective value of 140.7 meV^{-1} at T_C when the hyperfine coupling is included. This means that the two-ion coupling should be $\mathcal{J}_1(\theta) = 1/140.7$ meV $= 0.00711$ meV. The dipole contribution to this coupling is $16.848\mathcal{J}_D = 0.00733$ meV, which is *larger* than required. Hence the exchange terms reduce $\mathcal{J}_1(\theta)$ by 0.000 22 meV. The fit of T_C only requires one exchange parameter, but $\mathcal{J}_{12}$ is important because the free energies of the ferromagnetic A_1 phase and the antiferromagnetic one determined by $\overline{\overline{A}}_2$ (where the moments on the sublattices 2 and 4 are reversed compared to the phase observed) are nearly equal. The effective coupling parameter in the A_2 structure is

$$\mathcal{J}_2(\theta) = 2\mathcal{J}_{13}\cos 2\theta - 2\mathcal{J}_{12} + 17.305\mathcal{J}_D \tag{18}$$

hence $\mathcal{J}_{12}$ is important for determining the energy difference between these two structures. A comparison of (17) and (18) shows that $\mathcal{J}_{12}$ has to be larger than 0.000 05 meV or the ferromagnetic phase would be unstable. In the case of $\theta = -25°$, the A_1 phase is slightly more stable than the A_2 phase even if $\mathcal{J}_{12} = 0$ (the corresponding dipole contributions are $17.595\mathcal{J}_D$ in (17) and $16.559\mathcal{J}_D$ in (18)). However, in both cases the difference in energy between the two excitations that have the same symmetry as the A_1 and A_2 phases is very sensitive to the value of $\mathcal{J}_{12}$. Deriving this parameter from the excitation energies observed at 1.6 K, we may determined the final value of the total exchange constant from T_C, and the result is

$$\mathcal{J}_{13} = -0.000\,64 \text{ meV} \qquad \mathcal{J}_{12} = \begin{cases} 0.000\,30 \text{ meV} & \theta = +25° \\ 0.000\,13 \text{ meV} & \theta = -25°. \end{cases} \tag{19}$$

The mean-field model fits the paramagnetic properties of the system reasonably well. However, as seen in figure 5, the calculated heat capacity in the ordered phase is somewhat smaller than that measured. The same applies to the ordered moment, as shown in figure 8. The maximum magnitude of the Ho moments was determined by Brown *et al* (1990) to be $5.7\mu_B \pm 0.2\mu_B$ (at 70 mK). The calculated value of the zero-temperature angular moment along the x axis is 3.82, corresponding to a moment of 4.8 μ_B, about 16% smaller than observed. The hyperfine interaction at zero temperature, where the nuclear moment attains its saturation value, is equivalent to a field of 1.63 kOe along the local x axis, corresponding to a field of 1.8 kOe along the a direction. At this field, the calculated a axis magnetization curve at 1.6 K lies 0.7–0.8μ_B below the experimental one, which is about the same as the above difference of $0.9\mu_B$ multiplied by $\cos\theta$. Hence, the two discrepancies are consistent with each other. The failure in the fit of the magnetization at 1.6 K occurs

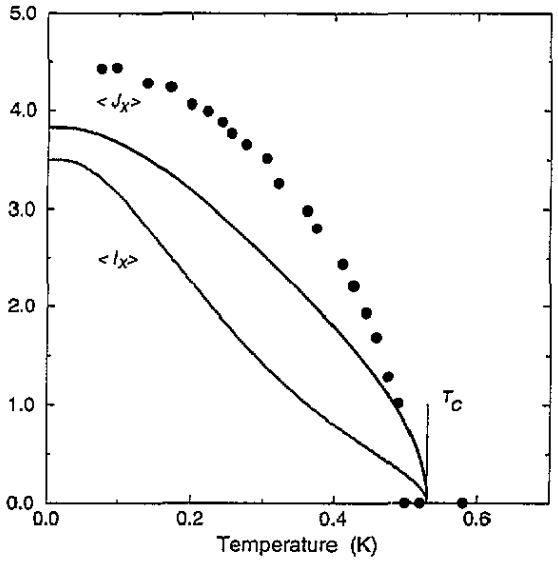

Figure 8. The solid lines show the calculated values of the angular moment $\langle J_x \rangle$ and the nuclear spin $\langle I_x \rangle$ of an Ho ion as functions of temperature below T_C. The filled circles are the experimental values of $\langle J_x \rangle$ derived from the variation of the magnetic scattering intensities at (1 0 0) obtained by Brown *et al* (1990). Their results have been scaled to agree with the magnetic moment of $5.7\mu_B$, which they obtained from structure refinements at 70 mK.

only at intermediate fields, the comparison is good both at low field (the susceptibility) and at high fields.

The (1 0 0) diffraction peak has been studied by neutron scattering in the ordered phase at 200 mK, as a function of field applied along the c axis. The integrated intensity decreases continuously until it nearly vanishes at a field of about 8.2 kOe. The model predicts that the c-axis field produces a continuous deformation of the zero-field A_1 phase until, at the critical field, it is changed into the A_3 structure, and the calculated field dependence of the (1 0 0) diffraction peak agrees qualitatively with the observed behaviour. However, the calculated critical field of 5.7 kOe is somewhat smaller than the experimental value.

4. The excitations

The RPA theory for the excitations is straightforward, except for the complication that the system consists of four magnetic sublattices. The frequency-dependent susceptibilities of the single ions in the mean-field approximation are the four $\overline{\overline{\chi}}_r^0(\omega)$ defined with respect to the global coordinate system, with the simplification that the ions on sublattices 1 and 2, or on sublattices 3 and 4, are magnetically identical. At zero frequency, the mean-field susceptibilities are replaced by the effective values as determined by (4), but as soon as the frequency is non-zero the nuclei have no effects on the response functions. The spatial Fourier transforms of the final susceptibility-tensor components, $\overline{\overline{\chi}}_{rs}(q, \omega)$, are defined similarly to (9), and the characteristic 12 × 12 coupling matrix may be written

$$\overline{\overline{\mathcal{M}}}(q,\omega)=\begin{pmatrix}\overline{\overline{\chi}}_1^0(\omega)\overline{\overline{\mathcal{J}}}_{11}(q) & \overline{\overline{\chi}}_1^0(\omega)\overline{\overline{\mathcal{J}}}_{12}(q) & \overline{\overline{\chi}}_1^0(\omega)\overline{\overline{\mathcal{J}}}_{13}(q) & \overline{\overline{\chi}}_1^0(\omega)\overline{\overline{\mathcal{J}}}_{14}(q)\\ \overline{\overline{\chi}}_2^0(\omega)\overline{\overline{\mathcal{J}}}_{21}(q) & \overline{\overline{\chi}}_2^0(\omega)\overline{\overline{\mathcal{J}}}_{22}(q) & \overline{\overline{\chi}}_2^0(\omega)\overline{\overline{\mathcal{J}}}_{23}(q) & \overline{\overline{\chi}}_2^0(\omega)\overline{\overline{\mathcal{J}}}_{24}(q)\\ \overline{\overline{\chi}}_3^0(\omega)\overline{\overline{\mathcal{J}}}_{31}(q) & \overline{\overline{\chi}}_3^0(\omega)\overline{\overline{\mathcal{J}}}_{32}(q) & \overline{\overline{\chi}}_3^0(\omega)\overline{\overline{\mathcal{J}}}_{33}(q) & \overline{\overline{\chi}}_3^0(\omega)\overline{\overline{\mathcal{J}}}_{34}(q)\\ \overline{\overline{\chi}}_4^0(\omega)\overline{\overline{\mathcal{J}}}_{41}(q) & \overline{\overline{\chi}}_4^0(\omega)\overline{\overline{\mathcal{J}}}_{42}(q) & \overline{\overline{\chi}}_4^0(\omega)\overline{\overline{\mathcal{J}}}_{43}(q) & \overline{\overline{\chi}}_4^0(\omega)\overline{\overline{\mathcal{J}}}_{44}(q)\end{pmatrix}. \tag{20}$$

Within the RPA we then find that

$$\begin{pmatrix}\sum_s \overline{\overline{\chi}}_{1s}(q,\omega)\\ \sum_s \overline{\overline{\chi}}_{2s}(q,\omega)\\ \sum_s \overline{\overline{\chi}}_{3s}(q,\omega)\\ \sum_s \overline{\overline{\chi}}_{4s}(q,\omega)\end{pmatrix}=\left[\overline{\overline{1}}-\overline{\overline{\mathcal{M}}}(q,\omega)\right]^{-1}\begin{pmatrix}\overline{\overline{\chi}}_1^0(\omega)\\ \overline{\overline{\chi}}_2^0(\omega)\\ \overline{\overline{\chi}}_3^0(\omega)\\ \overline{\overline{\chi}}_4^0(\omega)\end{pmatrix} \tag{21}$$

and the final susceptibility, determining the scattering cross-section , is

$$\overline{\overline{\chi}}(q,\omega)=\frac{1}{4}\sum_{rs}\overline{\overline{\chi}}_{rs}(q,\omega) \tag{22}$$

in terms of which the scattering function is

$$S(\kappa,\omega)=\frac{1}{\pi}\frac{1}{1-\mathrm{e}^{-\hbar\omega/kT}}\sum_{\alpha\beta}(\delta_{\alpha\beta}-\hat{\kappa}_\alpha\hat{\kappa}_\beta)\left[\overline{\overline{\chi}}''(\kappa,\omega)\right]^{\alpha\beta} \tag{23}$$

where $\hat{\kappa}_\alpha$ is the α component of the unit vector along the scattering vector κ.

The calculated excitation energies at 1.6 K, using the parameters defined in the preceding section, are compared with the experimental results in figures 9 and 10. The dispersion relations are symmetric with respect to the Brillouin-zone boundaries shown by the vertical dashed lines in the figures. There is a single degree of freedom per ion (the singlet–singlet transition), and the presence of four Ho ions per unit cell implies four magnetic excitations at each value of q. Along the high-symmetry directions $(h\,0\,0)$ or $(0\,0\,l)$, an effective double-zone representation is valid, implying that only two modes are visible in one scan. The representation is called effective, because it involves 180° changes of the phase of the c-polarized excitations to compensate for the difference between the (1,2) and (3,4) sublattices. The response function was also studied along $(h\,0\,1)$ and $(1\,0\,l)$, which leads to the same excitation energies as along $(h\,0\,0)$ and $(0\,0\,l)$ respectively. However, the response from the corresponding points in the double-zone representation is mixed to some extent. This is also the case in the scans along $(0\,k\,1)$ shown in figure 10, but the two branches indicated by the dashed lines are calculated to be so weak that they should not be visible. The variation of the scattering intensities, predicted by equation (23), is found to agree well with observation. To a very good approximation, only the xx component of the local susceptibility is non-zero, and one simple consequence of this is that the ratio between the intensities in $(0\,0\,l)$ scans and $(h\,0\,0)$ scans should be about $\cos^2\theta/\sin^2\theta = 4.6$, which is found to be the case (see figure 3).

The close agreement between experiment and theory, for both the excitation energies and the scattering intensities, allows a definitive identification of the different modes. These

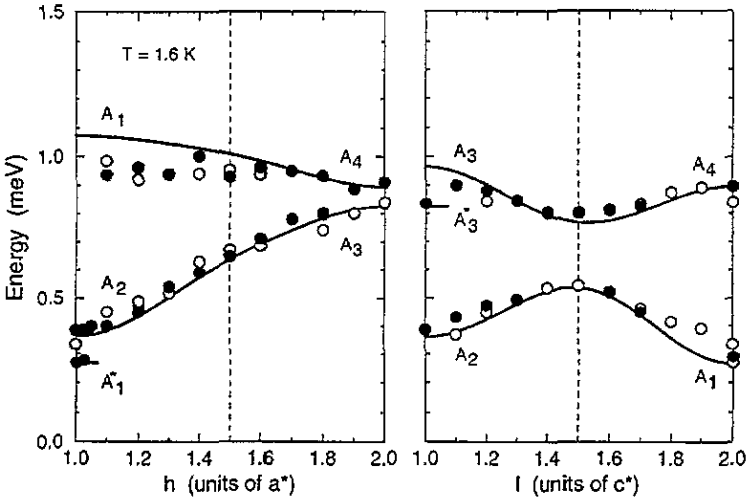

Figure 9. The dispersion relation of the singlet–singlet excitations along a^* and c^* in the paramagnetic phase of HoF_3 at 1.6 K. The closed circles are the experimental results obtained with the neutron-scattering vector along $(h\,0\,0)$ and $(0\,0\,l)$, whereas the open circles are the results obtained along the energetically equivalent directions $(h\,0\,1)$ and $(1\,0\,l)$ (with h and l lying between zero and unity). The results are shown in a double-zone representation, and the dashed lines indicate the Brillouin-zone boundaries. The solid lines are the theoretical predictions. They are labelled A_1–A_4 close to the Bragg points, which four modes corresponds to the four eigenvalues of the coupling matrix at zero wave-vector (15). The short solid lines marked A_1^* and A_3^* show the energies of the two ferromagnetic modes in the long-wavelength limit when the direction of the wave-vector is perpendicular to $(h\,0\,0)$ and $(0\,0\,l)$ respectively. In combination with the non-zero experimental resolution width, the A_1^* mode in particular contributes much more strongly to the scattering cross-section than the A_1 mode close to $(1\,0\,0)$. Notice that the ferromagnetic modes near $(2\,0\,0)$ and $(0\,0\,2)$ are the low-energy excitations that dominate the scattering cross section.

modes are labelled A_1–A_4 near the Bragg points, corresponding to the four different uniform structures predicted by the coupling matrices $\overline{\overline{A}}_1$–$\overline{\overline{A}}_4$ in (15). The modes near the Bragg points, which are transversely polarized with respect to the neutron scattering vector, are

$(0\,0\,2)$: A_1 and A_4

$(0\,0\,1)$: A_2 and A_3

$(1\,0\,0)$: A_1 and A_2

$(2\,0\,0)$: A_3 and A_4.

The A_2 and A_4 phases are antiferromagnetic and the energies of the corresponding excitations behave continuously near the Bragg points (in all directions). The two other phases, A_1 and A_3 have a ferromagnetic component along the a and c direction respectively. This means that the energies and scattering intensities of these two modes depend rapidly on the direction of the wave-vector q between the Bragg point and a nearby scattering point. Near $(1\,0\,0)$, the A_1 mode attains the maximum excitation energy if q is along $(h\,0\,0)$, whereas it becomes the incipient soft mode in the limit of $q \to 0$ along all the directions perpendicular to $(h\,0\,0)$. Because of the finite experimental resolution, this means that, close to $(1\,0\,0)$, the low-energy A_1 mode (indicated by an asterisk in figure 9) contributes

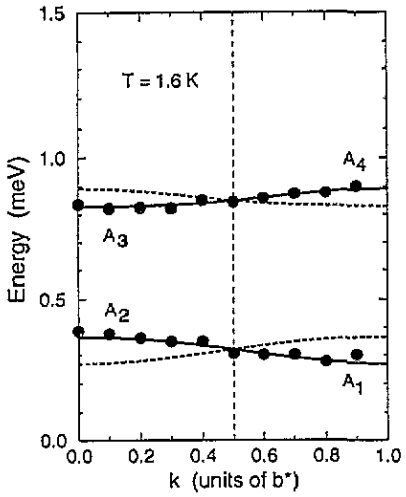

Figure 10. The excitation energies along b^* in the paramagnetic phase of HoF_3 at 1.6 K. The closed circles are the experimental results obtained along $(0\,k\,1)$, and the solid lines are the calculated results. The thick dashed lines indicate the excitation branches of much weaker scattering intensities. The different modes are labelled in the same way as in figure 9.

much more strongly to the scattering cross-section than the high-energy mode although the nominal scattering vector is along $(h\,0\,0)$. This tendency is much enhanced by the behaviour of the scattering intensities; close to $(1\,0\,0)$ the A_1 mode is weak whereas the A_1^* mode has high intensity. The experimental manifestation of this singular behaviour is illustrated by figure 2; the intensity of the low-energy A_1^* mode is large at $(1\,0\,0)$ but vanishes completely at the nearby scattering vector $(1.1\,0\,0)$. The A_1 mode along $(h\,0\,0)$ is still sensitive to the resolution width perpendicular to $(h\,0\,0)$ at $h = 1.1$, which may explain why the experimental energy and the scattering intensity of the mode at this point are smaller than calculated. The A_3 mode close to $(0\,0\,1)$ behaves in a similar way, except that the energy difference and the intensity variation are much smaller in this case, and in the comparison of the two A_3 modes the upper one has relatively more weight than found in the comparison between the two A_1 modes. The singular behaviour of the excitations near the Bragg points, which is a consequence of the long range of the dipole–dipole coupling, is very clearly demonstrated by the present system; similar effects have also been observed in holmium by Larsen *et al* (1987).

The incipient soft mode of the system is the low-energy A_1 mode at the Bragg points. At 1.6 K, which is well below $\Delta/k_B = 8.2$ K, the energy of this mode is close to its minimum value, which in the RPA is $\Delta\sqrt{1-\bar{R}}$. The mode stays at this energy (of about 0.27 meV) between 1.6 K and T_C. It does not become soft at the transition because of the additional nuclear contribution to the zero-frequency susceptibility. The other low-energy mode at the Bragg points is that corresponding to the ordered phase determined by $\overline{\overline{A}}_2$ in (15), and it is the one that is sensitive to the value of the coupling $\mathcal{J}_{12}$. If $\mathcal{J}_{12}$ were zero, this mode would lie slightly below the incipient soft A_1 mode in the case of $\theta = +25°$. $\mathcal{J}_{12}$ is the only fitting parameter that is not determined from the macroscopic behaviour of the system. This parameter is decisive for the determination of the energy difference between the A_1 and A_2 modes near the Bragg point, but it has little influence on the remaining part of the spectrum. The calculated excitation energies at 1.6 K are in good agreement with the observations. The only discrepancy of importance is shown by the A_1 mode when

approaching (1 0 0) along (h 0 0), which may to some extent be explained by the singular behaviour of this mode, in combination with the finite experimental resolution.

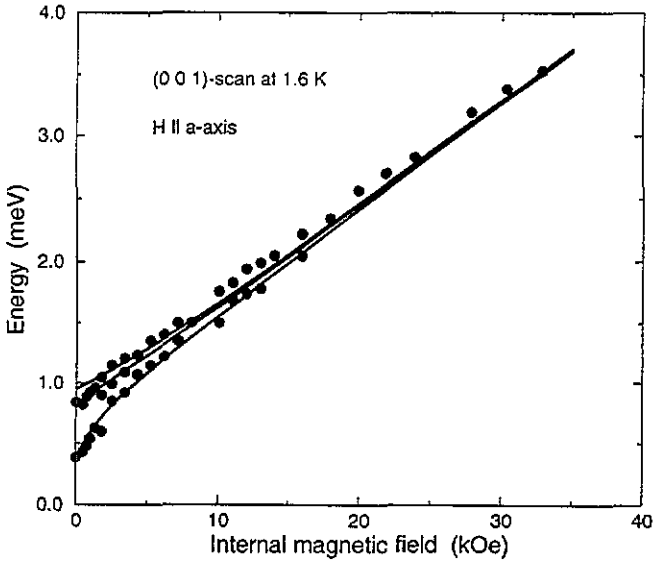

Figure 11. The position of the inelastic scattering peaks at (0 0 1) as a function of magnetic field applied along the a direction at 1.6 K. The circles are the experimental results and the solid lines show the calculated energies of the A_2, A_3^* and A_3 modes. Between 2 and 5 kOe all three modes are seen as separate peaks. The A_2 and A_3 modes are near the minimum and maximum excitation energies, and the decreasing distance between the two lines indicates that the total excitation bandwidth declines rapidly as the field is increased.

The (0 0 1) excitations have been studied at 1.6 K as a function of magnetic field applied along the a direction, and the result is shown in figure 11. The field adds to the singlet–singlet energy splitting and reduces the J_x-matrix element between the two states. This means that the excitation energies increase and that the scattering intensities and the amount of dispersion decrease, because of the field. The calculated energies are shown by the solid lines in figure 11 and compare well with the experimental ones. The same applies to the variation in the intensities. The amount of dispersion, as determined by the distance between the upper and lower line (the A_2 and the upper A_3 mode at (0 0 1)), is quickly reduced by the field, and above 30 kOe the excitation energies are very nearly constant throughout the zone.

The small scattering peak observed around 1.4 meV (at zero field at 1.6 K) is not accounted for by figures 9–11. As explained in section 2, this extra peak shows very little dispersion. Higher-order processes are relatively important in the large crystals used in these experiments, and the extra peak is interpreted as the result of double inelastic-scattering events. To a first approximation the dispersion of the singlet–singlet excitations may be neglected, in which case the secondary inelastic-scattered neutrons appear at every Q point compatible with an average energy of 2Δ transferred to the system. The dispersive effects will broaden this response, approximately as obtained from a convolution of the density of states of the singlet–singlet excitations with itself. The density of states is rather sharply peaked at the energy Δ, and the convoluted curve is estimated to be a Lorentzian-like curve centred at 2Δ with a width of about 0.5 meV. This compares well with the

observation. Furthermore, in the field experiment the extra peak behaved in accordance with this interpretation. The energy of the peak matched closely the field-dependent value of 2Δ, and the intensity decreased proportionally to the fourth power of the matrix element M.

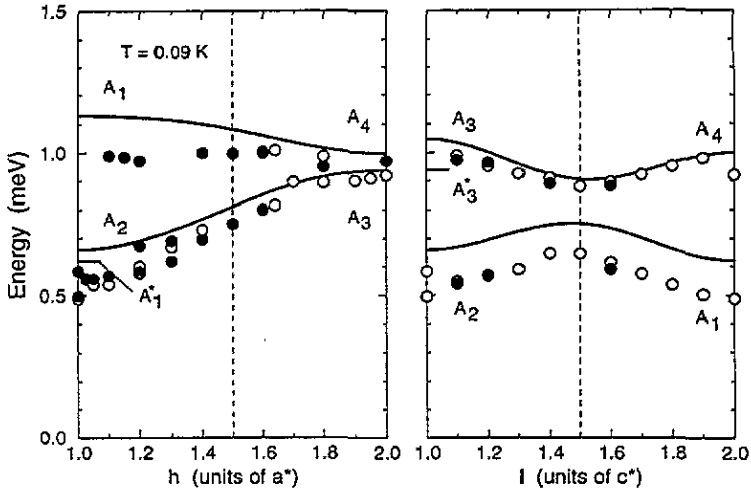

Figure 12. The dispersion relation along a^* and c^* in the ordered phase of HoF_3 at 90 mK. The meaning of the symbols is the same as in figure 9.

The dispersion relation was also studied in the ordered phase at 90 mK, at which temperature the nuclear moments are near their saturation value. The experimental results are compared with the calculated excitation energies in figure 12. The excitation spectrum is changed in the same way as if a field of about 1.8 kOe were applied along the a direction at temperatures just above T_C. This means that the excitation energies are increased, the intensities are decreased, and the excitation bands are flatter in comparison with the results at 1.6 K. The experimental results follow these trends, but not as pronouncedly as predicted by the model. The experimental low-energy bands lie clearly below the calculated ones, whereas the deviations at higher energies are less significant. The discrepancies between theory and experiments in figure 12 are surprisingly large, considering how well the paramagnetic excitations are described by the theory. They might be related to the other failure of the model, that the moment predicted in the ordered phase is too small, but the immediate consequence of this discrepancy is the opposite. An external field of about 1 kOe applied along the x direction at 90 mK leads to a calculated ordered moment close to the observed value, at which field the excitation energies are all predicted to increase by about 0.1 meV compared to the zero-field values shown in figure 12. Utilising the equivalence between the hyperfine field at 90 mK and a field of about 1.8 kOe at 1.6 K, we deduce that the field experiment in figure 11 indicates that the energy of the A_2 mode at (0 0 1) should be nearly 0.7 meV at 90 mK, whereas the observed energy is about 0.2 meV lower. This difference suggests that some of the large discrepancies in figure 12 may be due to experimental uncertainties. Although careful precautions were taken in order to ensure thermal equilibrium at 90 mK, the possibility that the actual sample temperature was higher cannot be excluded (the nuclear heat capacity is extremely large, about 10 J K^{-1} mol^{-1}, between 0.1 and 0.2 K). The experimental dispersion relation at 90 mK is explained by the

model, about as accurately as at 1.6 K, if the temperature of the crystals is assumed to be around 0.2 rather than 0.1 K.

All the calculated results presented are independent of the two possible choices given by (19). The calculated excitation energies are the same, but the intensities are predicted to differ to some extent in the two cases. However, the differences are not so characteristic or so large that they may be used for determining the sign of θ without very precise intensity measurements and a more complete theoretical model.

Discrepancies between theory and experiments are found whenever the moments are non-zero, as occurs in the ordered phase or in the presence of an external field. They may indicate either that the Hamiltonian is incomplete or that the mean-field/RPA is not sufficiently accurate. The Hamiltonian may contain quadrupole couplings between the ions, which would effectively change the crystal-field Hamiltonian when an external field is applied or the temperature is changed. The weakness of the two-ion couplings in the system indicates that the most likely possibility is that these couplings derive from the strain dependence of the crystalline field. We have tried to consider several possible magnetoelastic-interaction terms, and we found that they had to be rather large in order to produce the desired effects on the excitation energies. Their magnitude was then found to be incompatible with the macroscopic properties of the system; one underlying reason for this is that the induced dipole moments within the a–c plane do not introduce any new quadrupole moments. Further evidence against this explanation is that the measurements of the lattice parameters made during the neutron scattering experiments did not indicate any larger changes of these parameters. The other possibility is that the deficiencies of the model are due to correlation effects beyond the RPA. The inclusion of effects appearing in the next order of the $1/Z$ expansion (see for instance Jensen and Mackintosh 1991) will improve the comparison between theory and experiment; the only question is whether the corrections are large enough.

5. Conclusion

The excitation spectrum in holmium trifluoride has been investigated in a comprehensive way, both in the paramagnetic phase at 1.6 K, just above the ordering temperature, and in the ferrimagnetic phase at 90 mK. HoF_3 is in several aspects a unique system. At low temperatures, it may to a good approximation be treated as a singlet–singlet system. The local susceptibility of the ions is very anisotropic, though this Ising-like feature is not manifested directly in the bulk susceptibility, because there are four ions per unit cell characterized by two different magnetically easy axes. The two axes make the angles $+\theta$ and $-\theta$ with the a axis. The magnitude of the angle θ is known to be close to 25°, both from the neutron diffraction measurements of Brown *et al* (1990) and from the present analysis, but its sign is unknown. This uncertainty plays no role in the present analysis, because the magnetic asymmetry between the two cases is nearly completely disguised by an appropriate change of the exchange interaction $\mathcal{J}_{12}$ between next-nearest neighbours. It should be possible to determine the sign of θ by neutron diffraction. This would require scans in the $(h\,0\,l)$ scattering plane on a single magnetically ordered domain (in an applied field).

The classical dipole–dipole interaction dominates the two-ion dipole coupling, the exchange contributions are determined to be a factor of ten smaller. The two-ion coupling is about 0.86 times the threshold value for inducing magnetic ordering of the 4f moments. The hyperfine interaction between the electronic and nuclear moments leads to an enhancement

of the effective susceptibility and the coupled systems order cooperatively at 0.53 K. This behaviour is very similar to that observed in Pr metal. In Pr the critical ratio is 0.92, but, although this is closer to unity, the transition temperature is only about 0.05 K. The hyperfine interaction is relatively strong in both systems. The difference in the importance of the hyperfine coupling is an indirect consequence of the fact that the two-ion coupling in HoF_3 is much weaker than than in Pr. The critical ratio is then close to unity in HoF_3 only because the low-temperature susceptibility of the single ions is a factor of 20 larger than that in Pr. The large value of the electronic susceptibility implies that the Ho moments respond extremely sensitively to the hyperfine interaction.

The macroscopic properties of HoF_3 in the paramagnetic phase are accurately described by the mean-field model that has been developed; however the maximum moment predicted in the ordered phase is about 16% smaller than observed. The good agreement obtained between the calculated excitation energies and the observations in the paramagnetic phase gives strong support to the mean-field model. Nevertheless, the experimental excitation spectrum in the ordered phase differs significantly from the RPA prediction. One explanation for the discrepancies is that the ordered moments induce some magnetoelastic changes of the crystal-field Hamiltonian. Although it has not been analysed in full detail, experimentally or theoretically, the preliminary conclusion is not in favour of this possibility. Another explanation, which will be analysed in a forthcoming publication, is that the deviations are due to higher-order correlation effects. The marginal dimensionality is $d^* = 3$ (Als-Nielsen and Birgeneau 1977) and only logarithmic corrections of the mean-field behaviour are expected in the critical regime near T_C. This means that the higher-order correlation effects should be accounted for by the perturbative $1/Z$ expansion that has been applied in the case of Pr (Jensen and Mackintosh 1991). Preliminary calculations indicate that the introduction of the higher-order terms improves the fit to the high-energy part of the paramagnetic excitation spectrum and the fit to the paramagnetic heat capacity, but neither the calculated moments nor the excitation energies in the ordered phase are much affected.

Acknowledgments

The experimental work was financially supported by SERC. We are grateful to A Engesel for growing the crystals and to the staff at the Institut Laue–Langevin for the hospitality shown to us. We would like to thank B Bleaney and A R Mackintosh for a number of useful discussions and comments.

References

Als-Nielsen J and Birgeneau R J 1977 *Am. J. Phys.* **45** 554–60

Bleaney B 1972 *Magnetic Properties of Rare Earth Metals* ed R J Elliott (London: Plenum) p 383–420

Bleaney B, Gregg J F, Hill R W, Lazzouni M, Leask M J M and Wells M R 1988 *J. Phys. C: Solid State Phys.* **21** 2721–34

Bowden G J and Clark R G 1981 *J. Phys. C: Solid State Phys.* **14** L827–34

Brown P J, Forsyth J B, Hansen P C, Leask M J M, Ward R C C and Wells M R 1990 *J. Phys.: Condens. Matter* **2** 4471–84

Jensen J and Mackintosh A R 1991 *Rare Earth Magnetism. Structures and Excitations* (Oxford: Oxford University Press)

Larsen C C, Jensen J and Mackintosh A R 1987 *Phys. Rev. Lett.* **59** 712–5

Ram K and Sharma K K 1985 *J. Phys. C: Solid State Phys.* **18** 619–24

Sharma K K, Spedding F H and Blinde D R 1981 *Phys. Rev.* **24** 82–9